

GT2011-46294

THERMAL VALIDATION OF A HEAT SHIELD SURFACE FOR A HIGH LIFT BLADE PROFILE

M. Cochet, W. Colban, M. Gritsch, S. Naik and M. Schnieder

Alstom Power
Baden, Switzerland

ABSTRACT

Low emission requirements for heavy-duty gas turbines can be achieved with flat combustor temperature profiles, reducing the combustor peak temperature. As a result, the heat load on the first stage heat shield above the first stage blade increases. High lift airfoils cause increased thermal loading on the heat shield above the blade tip and impact the unavoidable secondary flows, including complex vortex flows.

Cascade tests have been performed on a blade with a generic high lift profile and the results on the heat shield are presented. A transient thermochromic liquid crystal measurement technique was used to obtain heat transfer coefficients on the heat shield surface. Several variations of blade tip clearance were investigated, and the impact on heat transfer coefficients is shown. Computational fluid dynamics predictions are compared to the experimental data to interpret the data and validate the CFD.

INTRODUCTION

The drive for lower pollutant emissions has many implications on gas turbine design. A homogeneous temperature profile at the combustor outlet has a strong potential for reducing emissions by lowering peak temperatures. However, this results in a higher thermal load for the endwalls of the turbine parts such as stator heatshields or vane platforms. In the past, endwall surfaces were protected by an increased amount of cooling air. Since the trend is to reduce cooling air to achieve higher efficiency, solutions have to be found to maintain the integrity of the endwall while using less cooling air. There is a strong need for a better understanding of thermal loads on endwalls.

A common issue of thermal loading on heat shield surfaces concerns the small gap between the tip of an unshrouded blade and the heat shield. The pressure distribution around the blade leads to an large pressure difference across the tip and to leakage of hot gas through the gap. This leakage has a strong

negative impact on the heat load of both the blade tip and the heat shield surface. This study focuses on the impact to the heat shield located right above the blade tip when subjected to this leakage flow. First, a literature review is given to define the scope of the study. Then the experimental study and CFD computations are described. The experimental and numerical results are aid in obtaining a better understanding of the flow features. Finally, the influence of the tip clearance on the heat transfer coefficients is shown.

NOMENCLATURE

G	Tip Gap Clearance [m]
C	Chord Axial Length [m]
H	Blade Span Height [m]
h	Heat Transfer Coefficient [$W/(m^2.K)$]
Nu	Nusselt Number [-]
P	Pressure [Pa]
P_i	Blade-to-BladePitch [m]
\dot{q}	Heat Flux [W/m^2]
Ma	Mach Number [-]
k	Thermal Conductivity
t	Time [s]
C_p	Pressure Coefficient

Abbreviations

CFD	Computational Fluid Dynamics
LE	Leading Edge
TE	Trailing Edge

TLC	Thermochromic Liquid Crystal
HTC	Heat Transfer Coefficients

Subscripts

<i>rec</i>	Recovery
<i>wall</i>	Wall
<i>ad wall</i>	Adiabatic Wall
<i>i</i>	Initial
<i>in</i>	Inlet
<i>out</i>	Outlet
<i>t</i>	Total

BACKGROUND

The blade tip leakage is a much-studied subject in the gas-turbine literature since it has a strongly negative impact on the stage efficiency, the aerodynamic losses, and the heat load over the blade tips and the heat shield surface.

Experimental studies made in low-speed cascade facilities have explained how the pressure difference across the blade tip generates a leakage flow from the pressure side to the suction side, and how this leakage flow interacts with the main air flow to produce the tip-leakage vortex (see for example Yamamoto [1]). **Figure 1** illustrates how the tip leakage flow and the tip leakage vortex are formed. Early studies have shown that the tip leakage is mainly due to the pressure distribution around the blade and not to the relative motion between the blade tip and shroud. The gap can be considered small enough so that the leakage flow between the tip and the shroud is largely one-dimensional and can be uncoupled from the details of the flow field (Metzger *et al* in [5]).

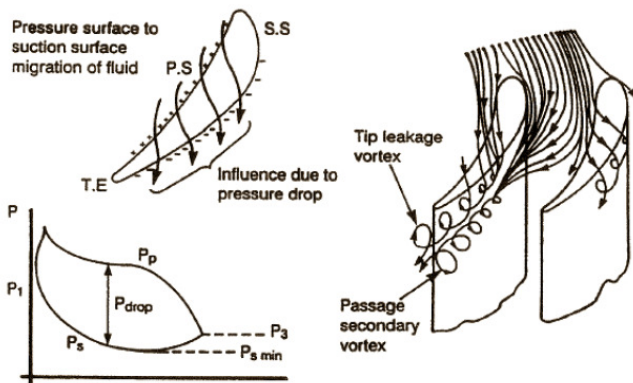


Figure 1: Formation of the tip leakage flow and tip leakage vortex (Harvey and Ramsden [2])

Several studies have dealt with the heat transfer resulting from the leakage flow, most of them focusing on the blade tip (Bunker *et al* [2], Ameri and Bunker [4]). While fewer studies have focused on the outer diameter casing surface, one of the first was a study by Metzger *et al* [5]. Using a full-stage rotating turbine and a shock-tube to generate short duration

sources of heat and pressurized air (the full experimental set-up is described by Dunn *et al* [6]), they measured the local time-resolved heat flux on the over-blade tip shroud. They proposed a 1D model based on the conventional boundary layer heat transfer correlation using the values of the relative gas-to-shroud velocity within the blade passage and increased the velocity by 10% to account for the periodic passage of the blade tip. Comparing their experimental results for the time-averaged heat fluxes to their 1D model, they obtained a fairly good agreement. It must be noted, however, that their results are only 1D and do not account for secondary flow features such as the tip leakage vortex. Last, the effects of temperature and heat transfer coefficients (aerodynamic effects) are not decoupled.

Rhee *et al.* [8] studied a stationary blade in a low-speed linear cascade. They used a naphthalene sublimation method to determine the local heat/mass transfer coefficients on the shroud surface. Several gap heights were tested and compared to a case without any gap. They found evidence that a strong heat transfer enhancement is observed along the tip leakage vortex path at the suction side. They also showed that the trajectory of the leakage flow moved away from the suction side as both the tip gap and the tip leakage increased. It must be noted that Rhee *et al.* [8] worked with a low-speed facility, which, according to Moore *et al.* [11], is inadequate in simulating the true flow structure in the tip gap.

Another experimental study was made by Kwak and Han [9] and investigated the effect of the tip crown geometry. Two geometries were compared; with and without a squealer along the pressure and the suction sides, as well as three values of the clearance-to-height ratio.

An experimental and numerical study by Naik *et al* [10], investigated the HTC on the endwall (or heat shield) surface above the blade using a generic blade tip with PS and SS squealer. They showed that cooling flow ejected from the blade has a relatively low impact on the HTC over the endwall surface, meaning that HTCs on the heat shield can be studied without any cooling flow. They also showed that HTCs on the endwall above the PS rim and the mid-squealer region is generally over-predicted by CFD compared to the experiments.

The effects of rotation are not considered in this paper. The periodic blade passing increases the relative velocity, which leads to an increase in heat flux by roughly 10% according to Metzger *et al.* [5]. Thorpe and Ainsworth [12] studied the heat transfer in the presence of periodic temperature fluctuations in more detail, showing that the time mean heat flux can be divided into a steady heat-flux (which can be studied in a stationary linear cascade) and an unsteady heat-flux, which depends on the periodic fluctuations of both the HTC and the adiabatic wall temperature. Based on this principle, they classify the overtip casing heat transfer experiments into two categories: (1) experiments designed to study the real engine conditions with full rotation and (2) simplified studies—such as those made in linear cascades—which are useful to investigate the impact of the blade tip design on the heat transfer. The

current study is of the second type. Additionally, the flows studied in the present investigations are generally subsonic.

MOTIVATION

This study investigated the local heat transfer coefficients on a stationary shroud with blade tip clearance and no coolant flow ejection from the blade. The heat transfer coefficients constitute the aerodynamic effects of the heat load. The focus of this study was the heat shield surface and not on the blade tip. There was no relative motion between the blade and the heat shield. Only the stationary heat transfer coefficients were investigated. The blade tip geometry that was investigated had both PS and SS squealers. The tip clearance G is the gap height between the top of the squealer rim and the heat shield surface, as illustrated in Figure 2. Three different tip clearances were tested in this study, as shown in Table 1. The clearance is normalized by the blade height H . The span to chord ratio is 1.32. Note that the terms “heatshield” or “shroud” are equivalent

Test case #	Small Gap	Nominal Gap	Large Gap
G/H	0.5 %	1 %	1.4 %

Table 1: Test matrix for tip clearance

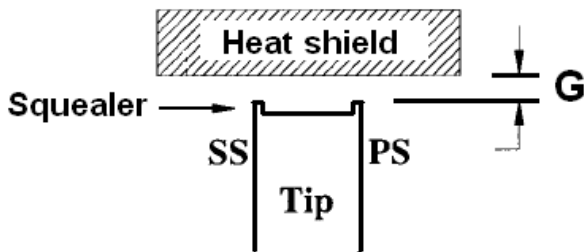


Figure 2: Geometry of the investigated zone

The geometric configuration presented in Figure 3 consists of a linear cascade of 3 blades. However, the focus is only on the pitch surrounding the center blade. The origin for the coordinate system is located at the blade leading edge. The Y -axis is in the tangential direction, and the X -axis in the axial direction. The Y -axis is normalized by the blade-to-blade pitch value, P_i , and the X -axis is normalized by the chord length C .

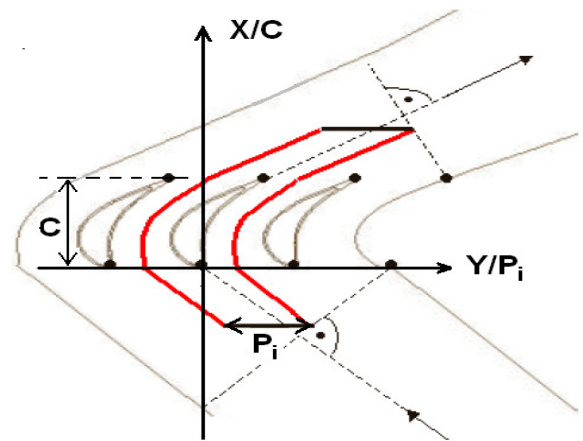


Figure 3: Geometric configuration

EXPERIMENTAL SET-UP

Cascade Test Bench

The experiments described here were performed in a high-speed, full-scale, open-loop wind tunnel at Alstom. The linear-cascade facility allowed for a representative Mach number distribution around the blade. More details on this test bench can be found in Krueckels *et al.* [13], Schnieder *et al.* [14] and Cochet *et al.* [15]. The wind tunnel featured a test section containing a four-passage linear cascade with an interchangeable test blade located at the center position (see Figure 4). Generic blades were used for the investigation..

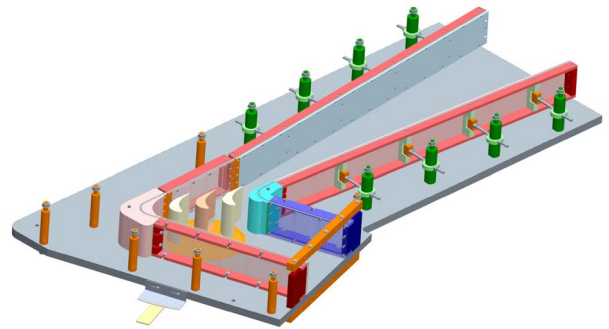


Figure 4: High-speed four-passage linear cascade

Above this test blade, a removable TLC Perspex cover was used to simulate the heat shield surface. This cover was used for the transient TLC HTC measurements. More details about both the cover and the transient TLC method are given in the following section.

Two two-stage radial compressors, capable of delivering up to 11kg/s of air to the wind tunnel at a total pressure of about 1.1bar, were used to simulate the hot gas flow. A 600kW electric heater featuring 19 individual heating elements was used to heat the main air. By specifying a supply voltage (0 to 10V), it was possible to heat the main air in the cascade in a

transient manner, with higher voltages corresponding to faster heat-up times. Due to the thermal properties of the Perspex hardware, an interlock was installed to disable the heater once the main air had reached a temperature of 70°C. Downstream of the heater, the air passed through a set of honeycombs and grids before entering the test section through an inlet nozzle, which accelerated the flow to its nominal velocity ($Ma_{in} = 0.43$). The turbulence intensity at the blade LE was approximately 5%, resulting from a turbulence grid located roughly 3.5 axial chord lengths upstream of the leading edge. At the TE of the blades, the flow reached a velocity of about $Ma_{out} = 0.85$. Downstream of the test section, the flow was decelerated through a diffuser section before being exhausted into the atmosphere through a silencer. Adjustable tailboards controlled the flow distribution through the four passages.

Transient TLC technique

The transient TLC technique used in this study is the step-change superposition method, which was used and described by Metzger and Larson [16], Hoffs et al. [17], Reiss et al. [18], and Vogel and Weigand [19]. In order to compute the heat transfer coefficients (h), the convective heat transfer equation must be solved,

$$\dot{q} = h(T_{rec} - T_{wall}) \quad \text{Eq. 1}$$

The classic solution to the 1-D transient energy equation with a step-change in temperature applied at time $T_i=0$ is:

$$\frac{T_{wall} - T_i}{T_{rec} - T_i} = 1 - \exp\left(\frac{h^2 \alpha t}{k^2}\right) \text{erfc}\left(\frac{h\sqrt{\alpha t}}{k}\right) \quad \text{Eq. 2}$$

Given the surface temperature (T_{wall}) at a given time (t), the local flow conditions (T_{rec}) and the initial conditions (T_i), one can solve for the heat transfer coefficients (h). However, if the true temperature history is not a step-change, but rather rises more gradually over time with an unspecified shape, as in the linear cascade, the above formulation is no longer valid. It is possible, however, using Duhamel's superposition theory, to reconstruct the true temperature history by supposing a series of incremental step changes in hot gas temperature.

$$T_{wall} - T_i = \sum_{j=1}^N U(t - \tau_j) \Delta T_{rec} \quad \text{Eq. 3}$$

The summation is evaluated at a given time (t), where t is the time integration variable, and ΔT_{rec} is the incremental change in T_{rec} from τ_{j-1} to τ_j . The function $U(t - \tau_j)$ is defined as:

$$U(t - \tau_j) = 1 - \exp\left(\frac{h^2 \alpha (t - \tau_j)}{k^2}\right) \text{erfc}\left(\frac{h\sqrt{\alpha (t - \tau_j)}}{k}\right) \quad \text{Eq. 4}$$

In effect, this method breaks down the temperature history into a summation of discrete step changes. If the temperature history of the free stream and the surface are sampled at a constant

frequency, this method enables calculation of the HTC for any time history.

The goal was to provide spatially resolved values of the HTC, and therefore local data was required. For that purpose, the Perspex cover surface was coated with a narrow-banded TLC color (42°C activation temperature), which was used to indicate the surface temperature distribution during testing. The TLC color was applied directly to the inside surface and covered with flat black paint to provide a solid background for the images, as illustrated in **Figure 5**. Optical access was provided through the Perspex heat shield model. The pictures were then spatially transformed in order to accurately represent the true surface distance and orientation.

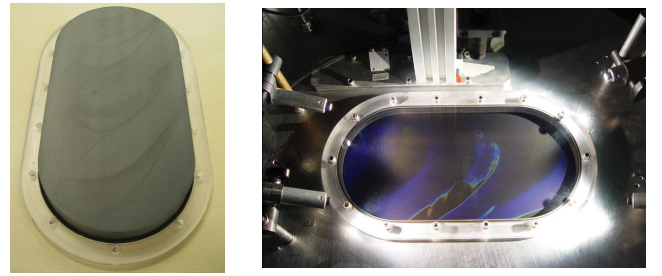


Figure 5: TLC-layered removable cover outside of the test rig (left) and during the tests (right)

The testing surface was brought to a thermal steady-state with a constant low temperature (roughly 303K) freestream flow. Then, the freestream temperature was increased as quickly as possible using a heater at time $t=0$. Video sequences of the surface TLC color response were recorded using a 25Hz miniature CCD camera mounted above the test rig. The time until each point on the surface reaches the TLC activation temperature was extracted from the video footage. Finally the HTC values were computed from the data using the step-change superposition technique.

Each transient test lasted roughly 10 seconds, while typically only the first 4-5 seconds of the data was useful for post-processing, due to the time required for color changes to occur. The Perspex model was thick enough to neglect heat conduction issues.

Uncertainty analysis

The measurement uncertainty of the HTC results for the transient IR method was determined by the perturbation method presented by Moffat *et al.* [20], applied to Equations 2 and 3.

$$\Delta h = \sqrt{\left(\frac{\partial h}{\partial T_{rec}} \Delta T_{rec}\right)^2 + \left(\frac{\partial h}{\partial T_{wall}} \Delta T_{wall}\right)^2 + \left(\frac{\partial h}{\partial t} \Delta t\right)^2} \quad \text{Eq. 5}$$

The following uncertainties have been included:

- 1) $\Delta T_{rec} = \pm 0.2K$ (from earlier TLC measurements)
- 2) $\Delta T_{wall} = \pm 0.2K$ (TLC calibration)
- 3) $\Delta t = \pm 0.04s$: CCD camera acquisition frequency is 25Hz

Uncertainties were roughly 7.5% for a low values of HTC and around 15% for high values of HTC at representative conditions. The overall uncertainty was especially sensitive to the temperature uncertainty due to the nature of Equations 2 and 3. To solve for the HTC levels, it was necessary to rearrange Equation 2 and to search for a minimum. This was the source of most of the uncertainty, because the search was very sensitive to the temperatures values T_{rec} and T_{wall} . The uncertainties above represent a single test run at a single heater setting. For each test case, measurements were made at two different heater voltage settings, and the results were then averaged together. The average difference between HTC values in each test run was roughly 11.8%.

NUMERICAL SET-UP

A steady-state CFD simulation of the test rig configuration was set up with Fluent 6.3 to provide detailed information about the local three-dimensional pressure and velocity field around the blade tip that could not be obtained by measurements. Additionally, CFD was used to investigate the sensitivity of the HTC to changes in tip clearance and for comparison with experimental results.

While four blade passages are used to achieve periodic flow in the cascade, only one blade is modeled for the CFD studies, using a blade-centered approach. In the test rig, only the instrumented center blade featured a tip clearance. Modeling only one blade with periodic boundaries introduced a deviation from the test rig setup, because it is equivalent to all test rig blades having a tip clearance. However, the influence of this deviation on the results was considered negligible.

Unstructured hybrid meshes were created for all three clearances using Centaur 7.01. As this study aimed to evaluate heat transfer quantities, the boundary layer had to be completely resolved. This requires $y^+ \approx 1$, which could be achieved on the whole blade surface. On the heat shield, local y^+ values of up to 5 resulted from mesh quality requirements. Nevertheless, the “enhanced wall treatment” approach of Fluent is still valid in this range, meaning that the boundary layer is resolved down to the wall on the whole heat shield surface.

Figure 6 shows the distribution of y^+ on the heat shield surface. The y^+ values were less than 1 across the entire blade tip surface.

The hub wall was treated as an inviscid wall to reduce the mesh size. The impact of not modeling the hub wall boundary layer on the passage flow was tested and found negligible with respect to cascade inlet mass flow and inlet mach numbers as well as for blade mach numbers. As a result of a mesh sensitivity study, it was found that appropriate mesh sizes were on the order of 1 million cells, corresponding to a computing time of a few hours for a single simulation. The realizable k- ϵ turbulence model was used.

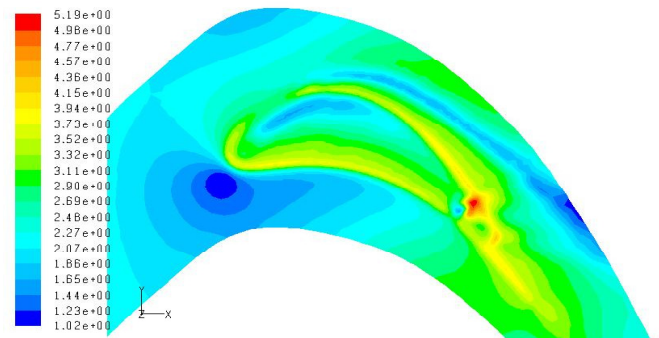


Figure 6: Distribution of y^+ on the heat shield surface of the final mesh

All boundary conditions were defined according to the test rig conditions. The only significant difference was the hot gas total inlet temperature. It was set to around 330-340K for the steady-state CFD simulations, while it varied for the experimental setup due to the transient measurement technique.

To account for recovery effects and for reasons of consistency with the experimental setup, the HTC was defined using the local adiabatic wall temperature. This requires that each measurement point be simulated twice:

1. with adiabatic walls
2. with a fixed wall temperature

The HTC can then be defined using the following equation:

$$h = \frac{\dot{q}}{T_{ad\ wall} - T_{wall}} \quad \text{Eq. 6}$$

$T_{ad\ wall}$ is the local adiabatic wall temperature determined by the first calculation. T_{wall} is the fixed wall temperature

boundary condition for the second calculation, and \dot{q} is the resulting heat flux from the second calculation. To avoid a change in the direction of the heat flux vector, the fixed wall temperature was set to 270K. This yielded a ΔT between hot gas and coolant total temperature of around 60K to ensure that the heat was always flowing from the surrounding fluid into the blade or heat shield material, respectively.

RESULTS

The pressure distribution on the heat shield wall was measured with static pressure taps and is compared to CFD in Figure 15. Shown is the pressure coefficient as defined in the following equation:

$$C_p = \frac{P_{t,in} - P}{\frac{1}{2} \rho_{in} u_{in}^2} \quad \text{Eq 7}$$

As far as the experimental resolution allows concluding, the pressures are predicted well. In the following part, Nusselt

numbers from both the numerical and the experimental study are compared. The Nusselt number is defined using the following equation:

$$Nu = \frac{h \times C}{k} \quad \text{Eq 8}$$

2D Nusselt distributions and flow structure

2D distributions of the Nusselt number on the heat shield surface are shown in Figure 7, Figure 8 and Figure 9, for both the numerical and experimental results.

Several flow features can be recognized.

- In the passages between the blades, lower Nusselt numbers can be observed for both the computations and the experiments. The CFD simulations seem to slightly overestimate the heat transfer coefficients in this region compared to the experimental results. Figure 11 shows a better representation of the passage distribution.
- At the blade LE, a small region of enhanced Nusselt number can be seen. This region is shown by the simulations and the experimental results for all clearance heights. For the smaller tip clearance, much higher values of Nusselt number can be seen. This is most likely due to stagnation at the leading edge coupled with the flow contraction within the tip gap.
- There is a rise in Nusselt number right above the PS squealer rim, which corresponds well to flow entrance effects and to the acceleration of the flow. This feature can also be seen in the results of Rhee et al. [8] and Kwak and Han [9]. The CFD tends to overestimate this increase in Nusselt on the squealer rim.
- Immediately downstream of the PS rim and parallel to it, a pair of features can be recognized as two consecutive zones, the first showing decreased Nusselt number, and the next showing increased Nusselt number. When the tip gap clearance was increased, the zone with lower Nusselt number grew in size while the zone with higher Nusselt was shifted towards the SS squealer rim. These features can also be seen in the results of Rhee et al. [8] and Kwak and Han [9]. These features were not well-captured by the CFD, which only shows a wider high-Nusselt zone with increasing gap height.
- Another zone of elevated Nusselt number occurs along the SS squealer and can be easily explained by the acceleration effect induced by the rim. This effect was observed by both the experiments and the CFD. This phenomenon was not seen by Rhee et al. [8], since no rim was used in their study. However, it is clearly visible in the results of Kwak and Han [9], which also featured double squealer rims.
- A final feature of interest runs along the suction side immediately downstream of the rim. This complex zone, which is composed of two regions of elevated Nusselt number that surround a region of lower Nusselt number, is caused by the tip leakage vortex. This zone begins at around 60% of the axial

chord. The increase in Nusselt number levels in this region with increasing gap size can be attributed to an increase in the leakage flow rate. This feature drifts away from the SS with increasing clearance (as was also observed by Rhee et al. [8]), however not as strongly for the experiments as for the CFD.

- With increasing tip gap height, the overtip leakage becomes much stronger (as shown in Figure 16). This increases the area of high Nusselt number above the blade tip. The vortex structures remain similar for all three gap sizes.

HTC measurements along streamlines

One of the purposes of the computational study was to gain a better understanding of the flow structures. Since CFD mimics several of the features recorded by the experiment, it can be used for a more in-depth analysis. Therefore, flow streamlines near the heat shield surface were used to compare numerical and experimental results. For each case, streamlines were extracted from the CFD computations along a surface located between the blade tip and the shroud. Along these streamlines, Nusselt number values were extracted from both CFD and experimental results. Three different streamlines were investigated, through the passage on the PS, through the passage on the SS following the tip leakage vortex, and following the leakage flow over the blade tip. Although the streamlines were not identical for each gap height, they were close enough between all three cases that they could be compared.

- The results for the PS streamlines are shown in Figure 10 in the left hand column. There is a good agreement between the CFD predictions and the experiments for all gap heights. It must be noted that the results do not vary much between the three gaps. As expected, the tip clearance does not seem to have a noticeable effect on the streamlines within the passage away from the tip vortex.

- The results for the streamlines directly following the SS are shown in the middle column of Figure 10. Except for the small tip gap case, there is a good qualitative agreement between CFD and experiments for all clearances for $X/C < 0.7$. In the TE region ($X/C > 0.7$), there is a sharp increase in the Nusselt number that is not captured by the CFD. This can be explained by the location of the tip leakage vortex being closer to the SS than what is predicted in the numerical results. Therefore, the numerical streamlines are likely misaligned with the true flow path, and cross into the tip leakage vortex for the experimental results, resulting in higher Nusselt number values.

- The streamlines corresponding to the leakage flow between the blade tip and the heat shield are presented in Figure 10 in the right hand column. The analysis was done along several streamlines that crossed through the tip gap region, with similar results for each. Therefore, only one is shown in Figure 10 for illustration. For the experimental results, three separate peaks can be identified. The first peak corresponds to the PS squealer rim location, with the Nusselt number remaining roughly the same for all test cases (around 2000). This is directly followed by a small zone where the

Nusselt levels drop, corresponding to an increase in area with increasing tip clearance. In the experimental results, this zone is followed by a second peak with high Nusselt values of up to 4000. However, the CFD predictions only capture a single peak and completely miss the local minimum in Nusselt number. This is all consistent with the 2D Nusselt number distributions, as well as the results of Rhee et al. [8]. As these authors pointed out, this complex feature could correspond to a transitional effect. Due to the acceleration of the flow close to the PS rim, the flow could be relaminarized, resetting the boundary layer, which would explain the first peak directly above the rim. Then the boundary layer would expand, leading to a sharp decrease in Nusselt number. Finally, the flow would transition to turbulent, triggering a second larger peak in Nusselt number. The final peak in Nusselt number along the shroud within the tip gap region corresponds to the location of the SS squealer rim. This peak—which increases with increasing clearance height in the experimental results—is well captured but clearly overestimated by the CFD. This effect could be explained by an increase in leakage flow.

Nusselt number levels within the blade passage

One conclusion from Metzger et al. [5] was that the heat transfer on the heat shield surface could be reasonably well predicted using a conventional turbulent boundary layer correlation:

$$St = 0.0296 \cdot Re_x^{-0.2} \cdot Pr^{-0.67} \quad \text{Eq. 8}$$

This correlation was applied to the current study by using the absolute gas velocities relative to the heat shield surface at several points: upstream of the blade LE, at the blade LE, at the blade TE, and downstream of the blade TE. The absolute velocities at these points were extracted from the CFD predictions, and a linear interpolation was used to obtain the velocity values between these locations.

The Nusselt number distributions along the blade passage from the experiments are compared to those computed using Equation 8 from the CFD velocity distribution in Figure 11. These Nusselt number distributions were then pitch-averaged and plotted for all three gap clearances, in Figure 12.

It can be noted that:

- Although the quantitative trend compares well to the experimental results, the CFD predictions overestimate the Nusselt number within the blade passage by roughly 25%.
- Two flow features can be recognized on both the CFD and the experimental curves. First, a small but sharp increase upstream of the blade LE, which can be explained as the stagnation at the LE. Second, there is a steady increase in Nusselt number starting at roughly $X/C = 0.6$. This increase is augmented with increasing gap clearance and can be attributed to the tip leakage vortex.
- The CFD predicts a strong decrease in Nusselt number upstream the blade LE, which is less pronounced in the

experiments and not captured at all by the correlation. The differences can be attributed to an underpredicted boundary layer thickness (i.e. a computational domain that was not long enough upstream the blade).

- The experimental results compare very well with the Sherwood number results from Rhee et al. [8]. However, they did not report a rise in the Nusselt number in the tip vortex region with increasing tip clearance.
- The Nusselt number levels obtained with the correlation match the experimental results quite well. The variation is within 10 to 15%, corresponding to the order of magnitude of the measurement uncertainty.

Although the correlation misses some important features of the flow (the stagnation at LE and the tip leakage vortex), it is important to note that the order of magnitude and the overall trend in Nusselt number are well captured by this simple 1D correlation.

2D Nusselt number distribution above the blade tip

Similar to the method described in the previous section, Nusselt number levels were computed using Equation 8 and the velocity profiles extracted from the CFD simulations and compared to the measured values in the region just above the blade tip (shown in Figure 13). The pitchwise-averaged values are then plotted in Figure 14. For the shroud region just above the blade tip, there is a poor agreement between the numerical and experimental results. This method strongly overestimates the Nusselt number along the PS squealer rim. Furthermore, the double peaks near the blade LE are also not captured using this method.

CONCLUSION

This study used both numerical and experimental methods to evaluate the impact of variations in tip gap clearance on heat shield Nusselt number levels using a blade tip with PS and SS squealers. The experimental results were validated by reproducing the effects reported by other authors. Although the CFD predictions showed similar trends as the experiments, they tended to overestimate the Nusselt number levels and miss some important flow features, especially directly above the blade tip. Variations in tip clearance height showed no effect on the flow within the blade passage apart from the tip leakage vortex. However, the tip leakage vortex showed an increase in Nusselt levels and tended to shift away from the suction side with increasing gap size. Above the blade tip, the tip clearance height had a noticeable effect. A local maximum in Nusselt number was observed just downstream of and parallel to the PS rim. This region was shifted away from the rim with increasing gap size. This effect created a larger zone of decreased HTC right downstream of the rim, and a smaller zone of elevated HTC closer to the SS squealer rim. This complex feature has also been observed by other investigators.

Within the blade passage, quantitative assessments show that the pitchwise-averaged Nusselt number along the axial direction can be reasonably predicted by the conventional 1D

correlation proposed by Metzger et al. [5], despite the presence of complex features like the tip leakage vortex.

ACKNOWLEDGEMENTS

The authors would like to thank Christian Kreienkamp for his work on the computational part and for his very enlightening discussions.

REFERENCES

- [1]. Yamamoto A., "Endwall Flow/Loss Mechanisms in a Linear Turbine Cascade with Blade Tip Clearance", ASME, *Journal of Turbomachinery*, vol.111, pp.264-275
- [2]. Harvey N.W.; Ramsden K., 2001, "A Computational Study of a Novel Turbine Rotor Partial Shroud", ASME *Journal of Turbomachinery*, vol 123, pp. 534-543
- [3]. Bunker R.S, Bailey J.C, Ameri A.A., "Heat Transfer and Flow on the First Stage Blade Tip of a Power Generation Gas Turbine Part I: Experimental Results", *Journal of Turbomachinery*, vol. 122, p.263-271
- [4]. Ameri A.A. and Bunker R.S, "Heat Transfer and Flow on the First Stage Blade Tip of a Power Generation Gas Turbine Part II: Simulation Results", *Journal of Turbomachinery*, vol 122, p. 272-277
- [5]. Metzger D.E., Dunn M.G., Hah C., 1991, "Turbine Tip and Shroud Heat Transfer", *ASME Journal of Turbomachinery*, vol 113, p.52
- [6]. Dunn M.G, Rae W.J, Holt J.L, 1984, "Measurement and analysis of Heat Flux Data in a Turbine Stage: Part I: Description of Experimental Apparatus and Data Analysis", *Journal of Engineering for Power*, 106, p.229-240
- [7]. Kumada M., Iwata S., Obata M., Watanabe O. , 1994, "Tip Clearance Effect on Heat Transfer and Leakage Flows on the Shroud-Wall Surface in an Axial Flow Turbine", ASME *Journal of Turbomachinery*, vol 116, p.39
- [8]. Rhee D.H., Choi J.H., Cho H.H., 2001, "Effect of Blade Tip Clearance on Turbine Shroud Heat/Mass Transfer" ASME Paper No. 2001-GT-0158
- [9]. Kwak J.S. and Han J.C, "Heat Transfer Coefficients on the Squealer Tip and Near Squealer Tip Regions of a Gas Turbine Blade", ASME *Journal of Heat Transfer*, Vol. 125, p. 669-677
- [10]. Naik S., Georgakis C., Hofer T. and Lengani D., 2010, "Heat Transfer and Film Cooling of Blade Tips and Endwalls", ASME Paper No. GT2010-23288
- [11]. Moore J., Moore J. G., Henry G. S., Chaudry U., 1989, "Flow and Heat Transfer in Turbine Tip Gaps", ASME *Journal of Turbomachinery*, Vol. 111, p 301-309
- [12]. Thorpe S. and Ainsworth R.W., 2008, "The Effects of Blade Passing on the Heat Transfer Coefficient of the Over-tip Casing in a Transonic Turbine Stage", *Journal of Turbomachinery*, vol. 130
- [13]. Krueckels J., Gritsch M., Schnieder M., 2009, "Design considerations and validation of trailing edge pressure side bleed cooling", ASME Paper No. GT2009-59161.
- [14]. Schnieder M., Parneix S., von Wolfersdorf J., 2003, "Effect of Showerhead Injection on Superposition of Multi-row Pressure Side Film Cooling with Fan-shaped Holes", ASME Paper No. GT2003-38693
- [15]. Cochet M., Arzel T., Gritsch M., Stephan B., Schnieder M., 2010, "High Temperature Turbine First Stage Vane Wake to Stator Heat Shield Interaction on Outer Heat shield", ASME Paper No. GT2010-22956
- [16]. Metzger D.E. and Larson D.E. , 1986, "Use of Melting Point Surface Coatings for Local Convection Heat Transfer Measurements in Rectangular Channel Flows with 90-deg Turns." ASME *Journal of Heat Transfer*, vol. 108.
- [17]. Hoffs A., Bölcs A. and Harasgama S.P., 1997, "Transient Heat Transfer Experiments in a Linear Cascade Via an Insertion Mechanism Using the Liquid Crystal Technique", ASME *Journal of Turbomachinery*, vol. 119, pp. 9-13.
- [18]. Reiss H., Bölcs A. and Drost U., 1998, "The Transient Liquid Crystal Technique Employed for Sub- and Transonic Heat Transfer and Film Cooling Measurements in a Linear Cascade", 14th Bi-annual Symposium on Measurement Techniques in Transonic and Supersonic Flow in Cascades and Turbomachines, University of Limerick, 3-5 Sept. 1998
- [19]. Vogel G. and Weigand B., 2001, "A New Evaluation Method for Transient Liquid Crystal Experiments", NHTC01-1511, 35th ASME National Heat Transfer Conference, Anaheim, USA.
- [20]. Moffat R.J, 1988, "Describing the Uncertainties in Experimental Results," *Experimental Thermal and Fluid Science*, vol. 1, pp. 3-17
- [21]. Bunker R., "Turbine Blade Tip Design and Tip Clearance Treatment". VKI LS 2004-02

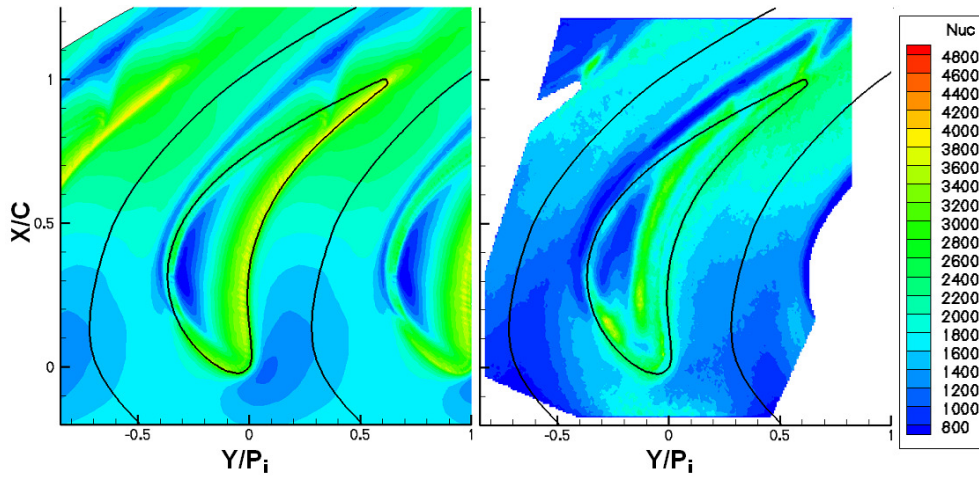


Figure 7: Small Gap: Nusselt number distribution for CFD (left) and measurements (right)

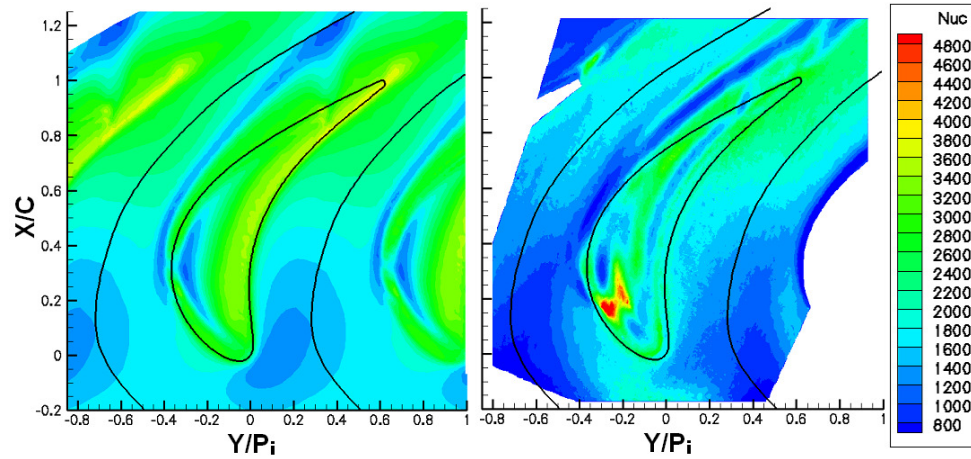


Figure 8: Nominal Gap: Nusselt number distribution for CFD (left) and measurements (right)

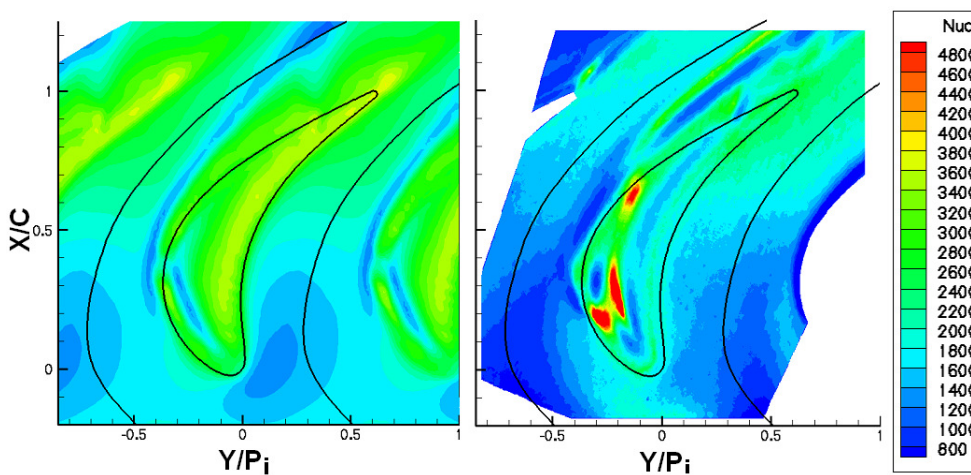
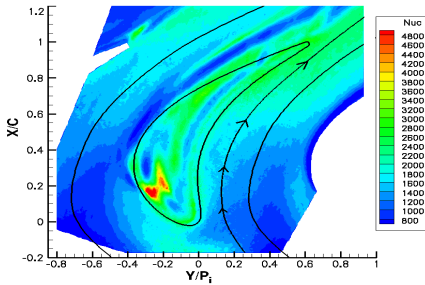
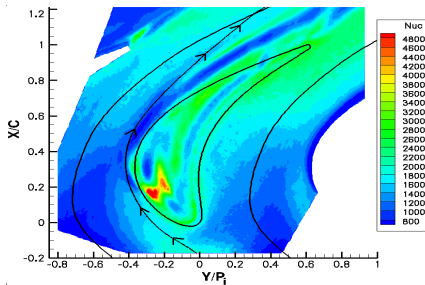


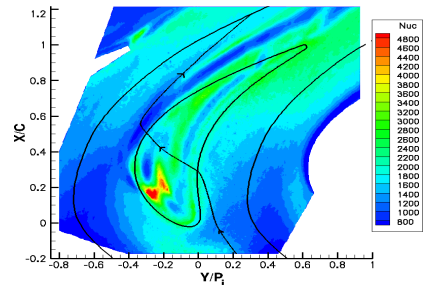
Figure 9: Large Gap: Nusselt number distribution for CFD (left) and measurements (right)



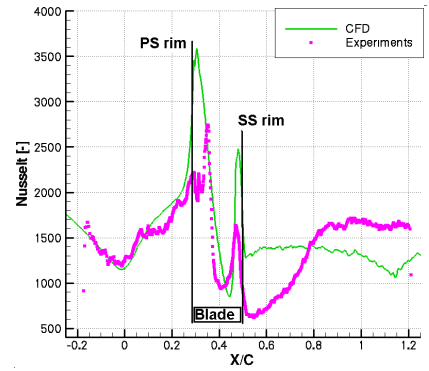
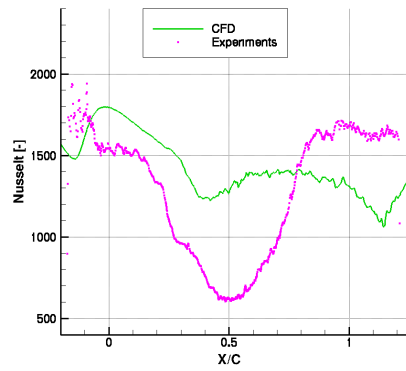
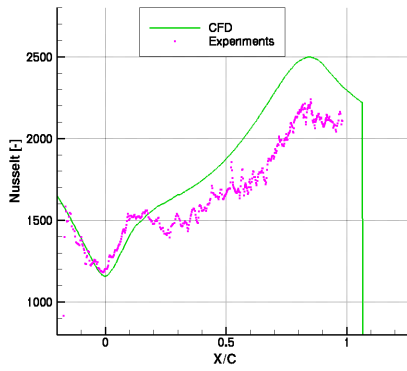
Streamline on the PS



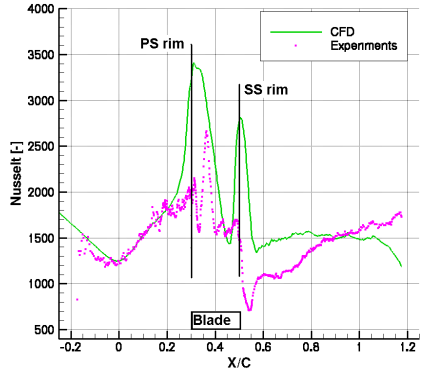
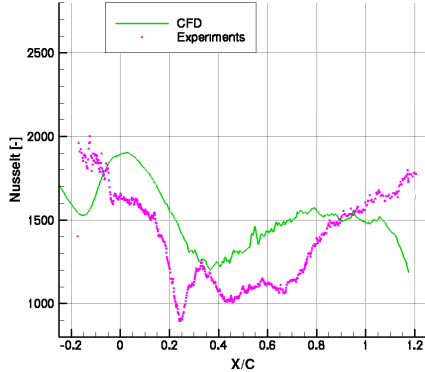
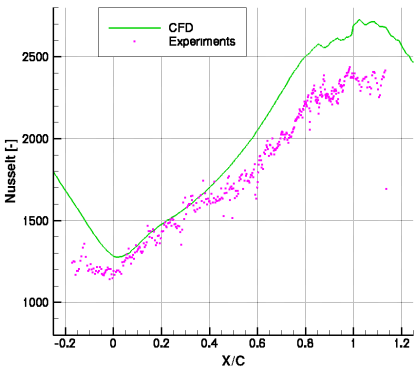
Streamline on the SS



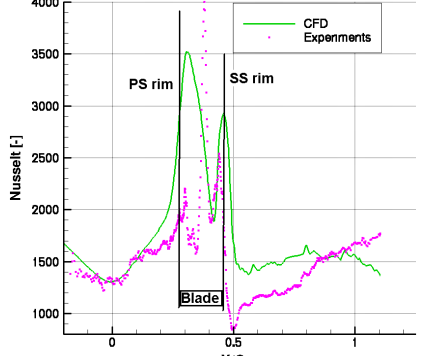
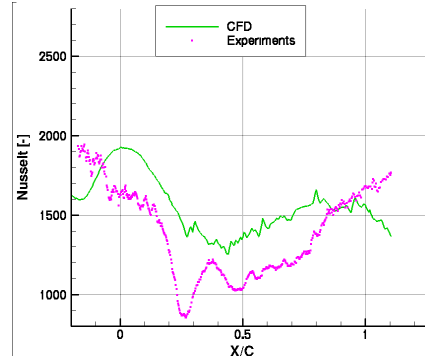
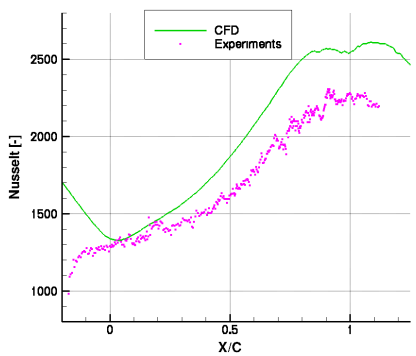
Streamline within the tip gap



Small Gap



Nominal Gap



Large Gap

Figure 10: Streamline comparison of Nusselt numbers on the PS, SS, and through the tip gap

Small Gap

Nominal Gap

Large Gap

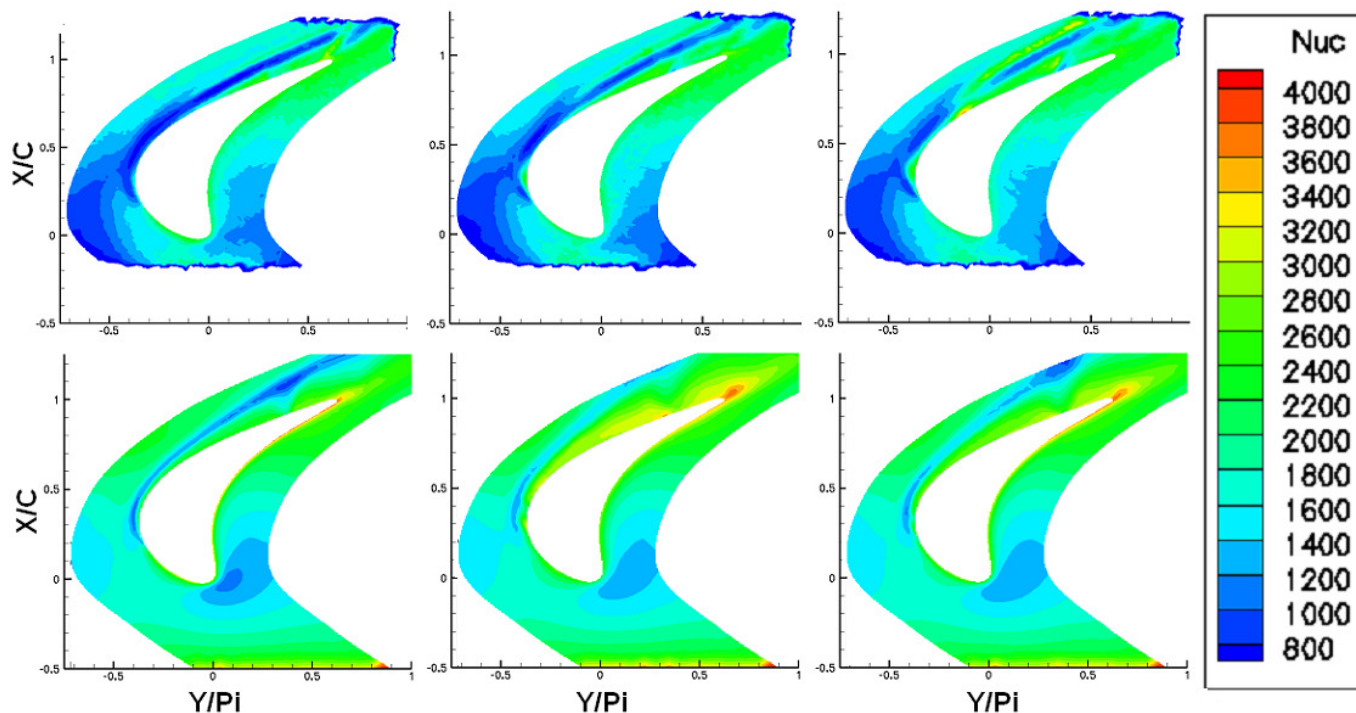


Figure 11: Nusselt number distribution within the blade- passage for the CFD (below) and the experiments (above)

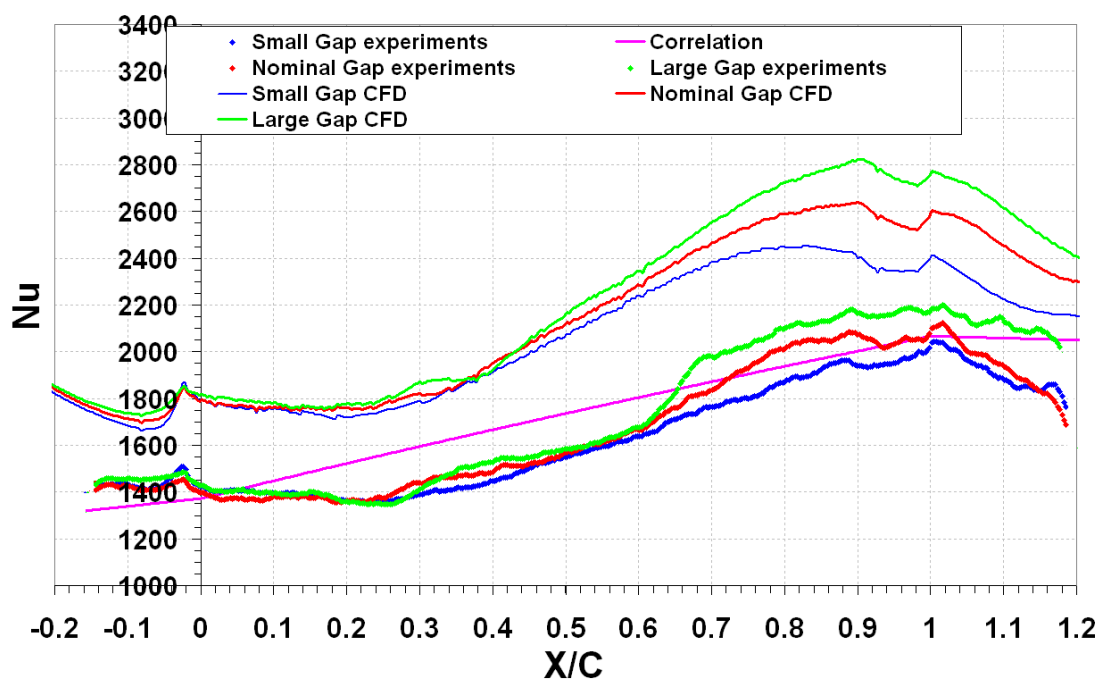


Figure 12: Pitchwise-averaged Nusselt number in the blade passage. Comparison between the CFD predictions, experimental results, and the 1D correlation

Small Gap

Nominal Gap

Large Gap

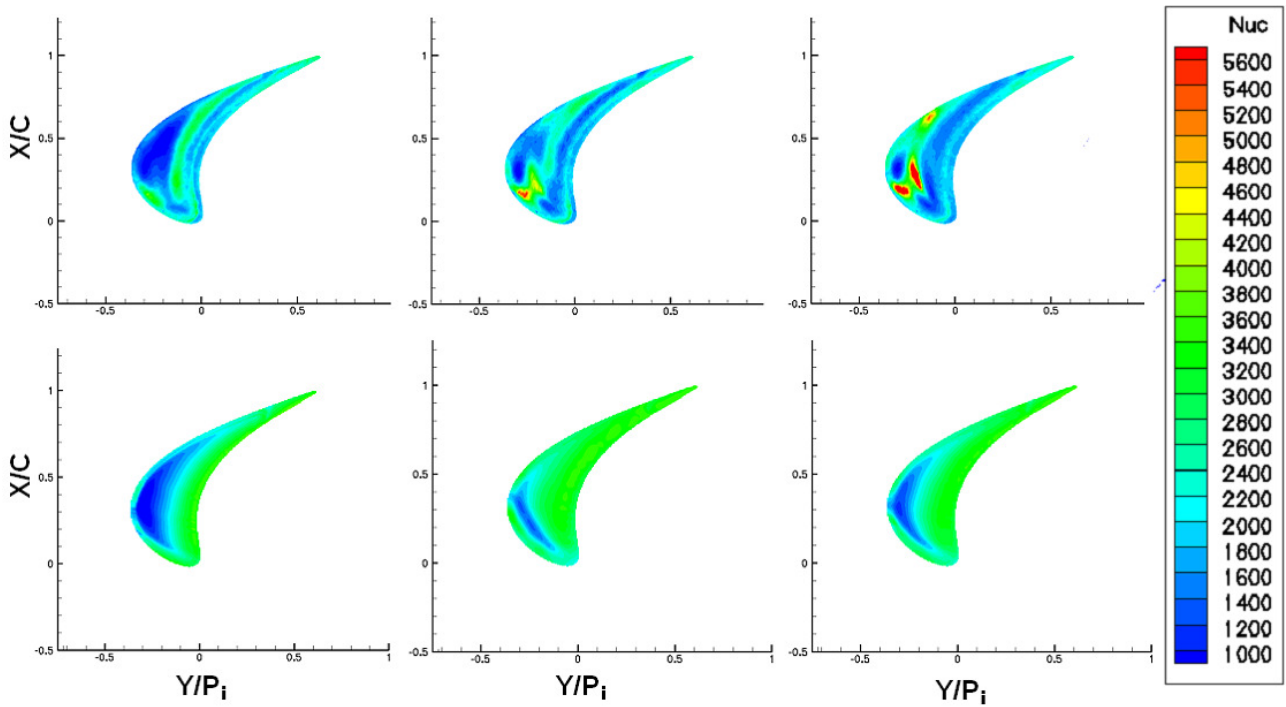


Figure 13: Nusselt number distribution on the heat shield surface above the blade tip for the CFD (below) and the experiments (above)

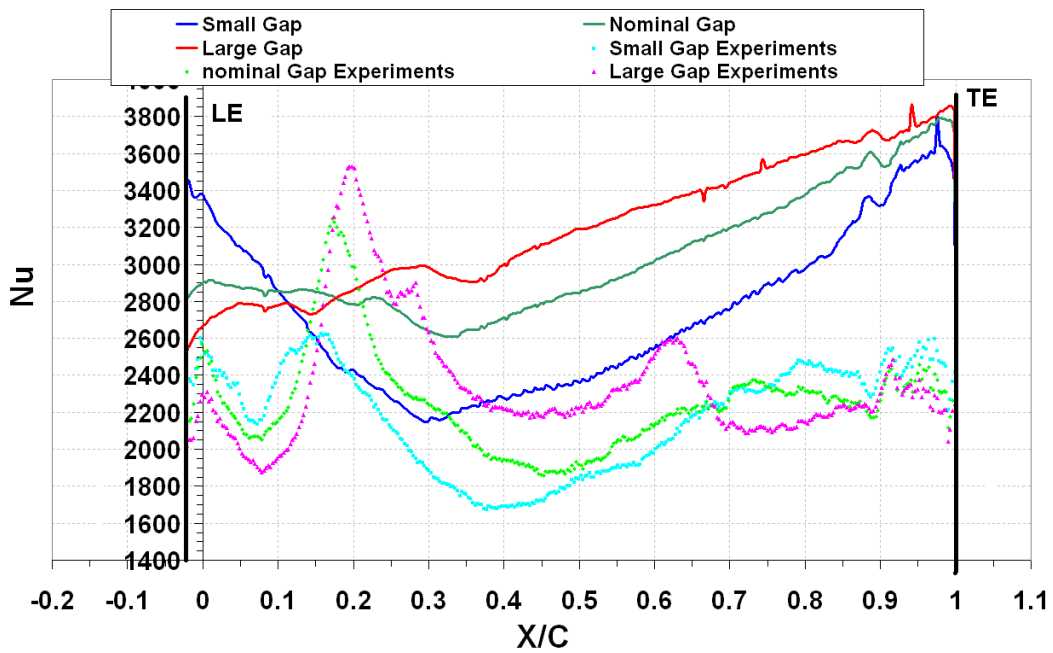


Figure 14: Pitchwise-averaged Nusselt numbers on the heat shield surface above the blade tip. Comparison between the numerical predictions and the experimental results

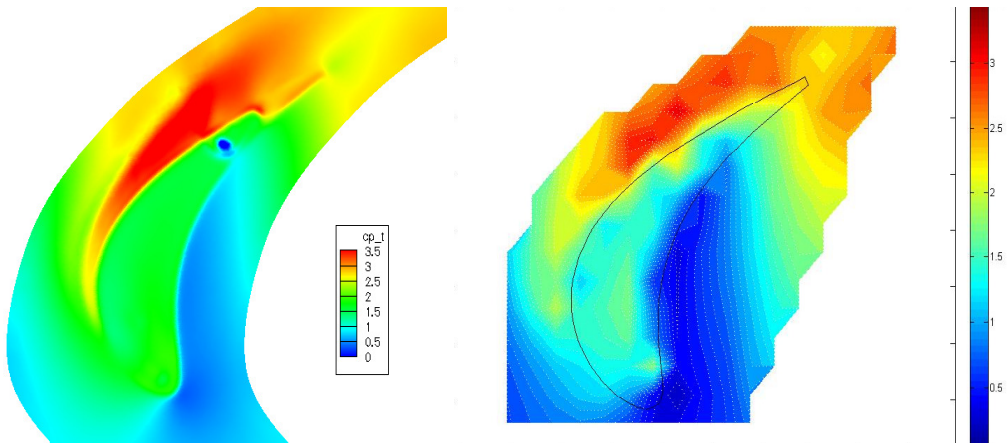


Figure 15 - Pressure coefficient C_p from CFD (left) and experiment (right)

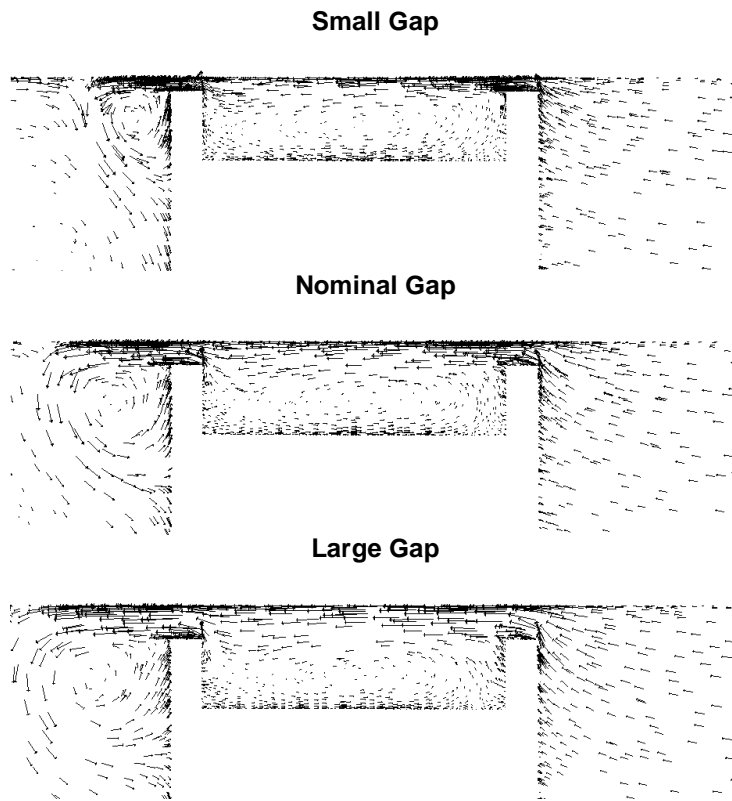


Figure 16: Vector plots showing flow structure within the tip gap